Ore Geology Reviews 104 (2019) 1–13

Contents lists available at ScienceDirect

Ore Geology Reviews

journal homepage: www.elsevier.com/locate/oregeorev

Giant bauxite deposits of South China: Multistage formation linked to Late Paleozoic Ice Age (LPIA) eustatic fluctuations

Shenfu Weng[a,b], Wenchao Yu[a,*], Thomas J. Algeo[a,c,d], Yuansheng Du[a,*], Peigang Li[b], Zhiyuan Lei[e], Shuang Zhao[b]

[a] State Key Laboratory of Biogeology and Environmental Geology, School of Earth Sciences, China University of Geosciences, Wuhan 430074, China
[b] 106 Geological Party, Guizhou Bureau of Geology and Mineral Exploration and Development, Zunyi 563099, China
[c] State Key Laboratory of Geological Processes and Mineral Resources, China University of Geosciences, Wuhan 430074, China
[d] Department of Geology, University of Cincinnati, Cincinnati, OH 45221-0013, USA
[e] Guizhou Bureau of Geology and Mineral Exploration and Development, Guiyang 550004, China

ARTICLE INFO

Keywords:
Glacio-eustasy
Karst
Karstification
Chemical weathering
Soil drainage
Chemical index of alteration

ABSTRACT

The Lower Carboniferous Jiujialu Formation bauxite deposits at Zunyi, northern Guizhou are distinguished by their great thickness (to 110 m) and cyclic alternation of bauxite ore and bauxitic claystone layers. These features are typical of the Kazakhstan subtype of karst bauxite deposits, although the genesis of this type of deposit is poorly understood. Here, we undertook a petrological, mineralogical, and geochemical study of the Zunyi deposit in drillcore ZK5600 to gain insights into its formation history. The Zunyi profile contains seven bauxite cycles, as recorded by petrological, mineralogical and geochemical features, indicating a multistage formation history. Each cycle is composed of a lower bauxitic claystone layer and an upper bauxite ore layer. The bauxite ore is characterized by high Al_2O_3, high Al-mineral (diaspore), and low SiO_2 content. Positive Ce anomalies, high CIA values (> 90), and strong depletion of major elements indicate that the bauxite ore formed through intense chemical weathering and leaching in a well-drained soil environment. The bauxitic claystone is characterized by relatively lower Al_2O_3 and higher SiO_2 and clay mineral (mostly illite) content. This lithology exhibits both negative and positive Ce anomalies, moderate CIA values (70–80), and enrichment of some elements (e.g., Fe, K), indicating formation through moderate chemical weathering in a poorly drained soil environment. Secular variations in chemical weathering intensity and soil drainage conditions were linked to regional hydrologic changes. During the early Carboniferous, the Zunyi area was located in a karstified coastal upland setting, and its hydrologic system was affected by glacio-eustatic fluctuations. High groundwater table elevations during eustatic highstands led to formation of bauxitic claystone layers, whereas low groundwater table elevations during eustatic lowstands led to formation of bauxite ore layers.

1. Introduction

Bauxite deposits are widely regarded as a reliable lithologic indicator of warm, seasonally wet climates (Bárdossy, 1994; Price et al., 1997; Retallack, 2010). However, bauxite formation is the product of an integrated set of environmental factors including climate, tectonics, eustasy, paleogeography, vegetation cover, and atmospheric circulation (Bárdossy, 1982; Bárdossy and Combes, 1999; D'Argenio and Mindszenty, 1995; Mindszenty, 2016; Yu et al., 2018). From the Carboniferous to the Permian, bauxite formation declined worldwide, which is usually ascribed to global climatic cooling linked to the Late Paleozoic Ice Age (LPIA) (Bárdossy, 1994; Bogatyrev et al., 2009). In contrast, the Permo-Carboniferous was the most important period for bauxite formation in China, and > 75% of present bauxite reserves in China date to this period (Gao et al., 2015). Increased Permo-Carboniferous bauxite formation in China implies the development of a unique combination of environmental factors in the eastern Paleo-Tethys region at that time.

Previous research on Jiujialu Formation bauxites focused mainly on Visean (early Mississippian) deposits in central Guizhou Province, where the bauxite ore is composed of aluminum oxide minerals (diaspore, α-AlOOH; boehmite, γ-AlOOH), clay minerals (kaolinite, illite), and iron oxide minerals (hematite) that exhibit an “iron-bauxite-coal” horizonation pattern from bottom to top (Liu, 1991; Cao et al., 2012; Ling et al., 2015, 2017). The source rock for these deposits is considered to have been underlying Ordovician shales and Cambrian dolostones.

* Corresponding authors.
E-mail addresses: yuwenchaocug@163.com (W. Yu), duyuansheng126@126.com (Y. Du).

https://doi.org/10.1016/j.oregeorev.2018.10.014
Received 12 July 2018; Received in revised form 8 October 2018; Accepted 19 October 2018
Available online 21 October 2018

This area experienced long-term exposure from the Late Ordovician to the Early Carboniferous (and possibly into the Early Permian), providing substantial time for bauxite formation. Ling et al. (2017) discussed the role of regional hydrogeology in the development of these deposits. They concluded that a rising groundwater table (GWT) led to pyrite-rich sediments covering the bauxite deposit. When the GWT fell and sediments were exposed to air, oxidation of pyrite led to formation of acids (e.g., H_2S, H_2SO_4) that enhanced leaching of Si and resulted in local Al enrichment.

In contrast, the bauxite deposits of the Jiujialu Formation in the Zunyi area of northern Guizhou Province have received much less attention. These deposits formed during the early-middle Visean (early Mississippian) and represent the oldest-known bauxite deposits of the South China Craton (Liu and Liao, 2012). Preliminary investigation revealed abrupt changes in deposit thickness (from 3 to 110 m) as well as the presence of multiple cycles of alternating bauxite ore and bauxitic claystone (or coal) layers (Weng et al., 2011; Liu and Liao, 2012; Liu et al., 2016). According to the classification of Bárdossy (1982), bauxite deposits formed on carbonate bedrock are 'karst bauxite', and the great thickness and ore-claystone cyclicity are typical of the Kazakhstan subtype of karst bauxite deposits.

This study focuses on bauxite deposits in the Lower Carboniferous Jiujialu Formation in the southern Zunyi area. To better understand the genesis of these deposits, we analyzed 97 samples from a 110-m-long drillcore (ZK5600) using petrographic, mineralogic, and geochemical techniques. Based on these data, we propose that formation of the Jiujialu Formation bauxites was controlled by cyclic changes in regional groundwater levels and climate conditions that were ultimately linked to glacio-eustasy and climate changes of the Late Paleozoic Ice Age (LPIA). This study thus provides new insights into the genesis of the Kazakhstan-subtype of karst bauxite ores.

2. Geological background

During the Carboniferous, the South China Craton was an isolated microcontinent located near the equator in the eastern Paleo-Tethys region (Fig. 1A; Yang et al., 2004; Zhu et al., 1998). Central Guizhou Province was a coastal area at that time, with shallow-sea areas to the south and continental areas to the north of a line running approximately through the city of Guiyang. Consequently, southern Guizhou accumulated a thick succession of Carboniferous marine carbonate deposits, central Guizhou was occupied by a low-elevation coastal karst plain with numerous sinkhole lakes, and northern Guizhou was a karstified upland. The continental environments in central and northern Guizhou are represented mainly by bauxite deposits that accumulated in sinkholes and dolines (Fig. 1B; BGMRGZP, 1987; Gao et al., 1992).

The study area is located in the southern Zunyi area of northern Guizhou Province, ~20 km east of Goujiang County (Fig. 1C). Cambrian and Cretaceous strata are present, but upper Cambrian/middle Ordovician to upper Devonian/upper Carboniferous strata are absent owing to a regional unconformity. This unconformity was generated by the late Ordovician Qianzhong Uplift, a tectonic unit in the central Guizhou area bounded by regional faults (i.e., the Zhengyuan-Guiyang Fault to the south, the Hezhang-Zunyi Fault to the north, and the Yadu-Ziyun Fault to the southwest) (Deng et al., 2010; Liu et al., 2011). The Qianzhong Uplift developed through re-activation of an older Ediacaran structure in response to far-field effects of the amalgamation of the Yangtze and Cathaysia blocks (the Guangxi Movement), resulting in long-term (> 100 Myr) subaerial exposure of central to northern Guizhou Province (Chen et al., 2001; Niu et al., 2007; Deng et al., 2010).

The bauxite deposits of the Jiujialu Formation in central Guizhou and the Zunyi area in northern Guizhou exhibit both similarities and differences. In both areas, the bauxite orebodies are found at subsurface depths of ~100 to 700 m, with control of their vertical distribution by a series of NNE-trending folds generated during the Late Triassic Indosinian and Jurassic Yanshan movements. In both areas, the underlying bedrock consists of the upper Cambrian Loushanguan Group (gray and white dolostone and silicic dolostone with a maximum thickness of ~900 m), the lower Ordovician Tongzi Formation (divided into a 20-m Lower Member composed of interbedded thin carbonate and mudstone layers, and a 30-m Upper Member composed of

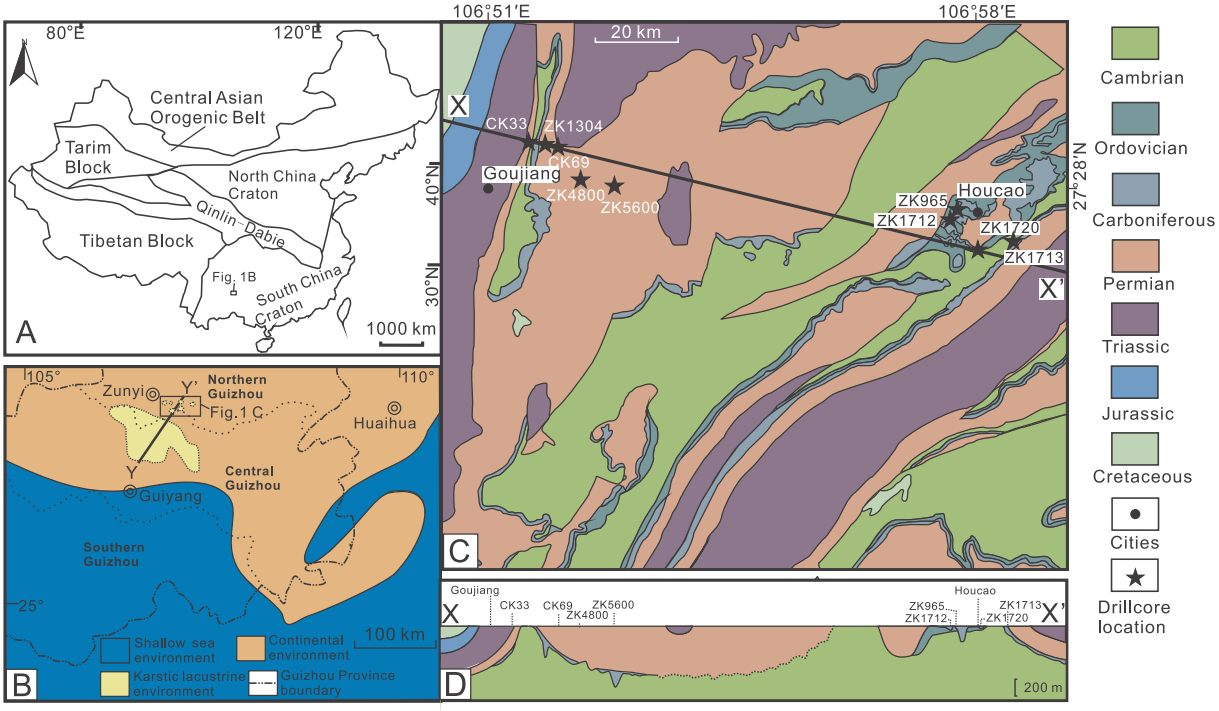

Fig. 1. (A) Location of the study area in China; (B) Paleogeographic map for Guizhou during the Carboniferous; (C) Geological map for Zunyi area, northern Guizhou; (D) Cross section X-X′.

limestone), and the lower Ordovician Meitan Formation (~20 m of gray and green shale and sandy shale with interbedded thin marlstone layers). Differences include: (1) Age of overlying units: the bauxite deposits in central Guizhou are conformably overlain by limestones and dolostones of the upper Visean-Bashkirian Dapu (or Baizuo) Formation but those in the Zunyi area are unconformably overlain by the Lower Permian Liangshan/Qixia formations. This pattern indicates that the late Mississippian transgression reached the central Guizhou area but did not reach the Zunyi area further to the north. (2) Composition of bauxite deposits: the lower ore member of the Jiujialu Formation is oxidized (hematitic) in central Guizhou but pyritic in the Zunyi area, and the upper ore member contains thin interbeds of bauxitic claystone at Zunyi but not in central Guizhou (Ling et al., 2017). (3) Thickness of bauxite deposits: ranging from ~2 to ~20 m with a mean of ~8 m in central Guizhou (Ling et al., 2015), and from ~3 m to ~110 m with a mean of ~30–40 m in the Zunyi area (Fig. 1C, 2).

Detailed palynological study has been undertaken on the ZK1304 drillcore, which is located ~ 18 km northwest of the ZK5600 drillcore (see Section 3) that is the focus of the present study (see Fig. 1C for locations). The 90-m-thick Jiujialu Formation was sampled for palynological study at four levels in the ZK1304 core: in the uppermost carbonaceous claystone layer, in two coal layers in the upper part of the core, and in an illitic claystone layer in the middle of the core (Liu and Liao, 2012). The palynological assemblages of these samples constrain the age of the Jiujialu Formation at ZK1304 to the early-middle Visean (Mississippian).

3. Materials

The present study is based on the ZK5600 drillcore (location coordinate: 27°28′3″ N, 106°54′14″ E), located ~25 km east of Goujiang County, in the Zunyi area of northern Guizhou Province (Fig. 1C). In this core, the Jiujialu Formation bauxite deposit overlies dolostones of the upper Cambrian Loushanguan Group and is overlain by limestones of the Lower Permian Qixia Formation. The thickness of the Jiujialu Formation in the study core is 110 m (depth 481–591 m). The bauxite deposit can be divided into 15 layers based on petrographic changes (see Table S1 for a detailed description). The lower 23 m is composed of bauxitic claystone, whereas the upper 87 m consists of seven bauxite ore layers ranging from 2.30 m to 14.21 m in thickness interbedded with thinner (1.00–7.10 m) bauxitic claystone layers. The bauxite ores exhibit clastic or massive textures and the bauxitic claystone exclusively massive texture. A total of 95 samples were collected from the bauxite deposit (Fig. 2), 62 from the bauxite ore (see Table S1 for details), and 23 from the bauxitic claystone layers. The sampling interval averaged ~1 m. In addition, one sample (ZK5600-95) was collected from the pyrite layer at the base of the Jiujialu Formation, one sample (ZK5600-96) from the underlying Cambrian Loushanguan Group dolostone, and one sample (ZK5600-1) from the overlying Permian Qixia Formation marlstone.

Logging data of eight drillcores in the vicinity of drillcore ZK5600 were collected for stratigraphic correlation, generating a 70-km WNW-ESE cross-section through the study area (Fig. 1C, 2). The thickness of the Jiujialu Formation shows rapid variations in these drillcores. In the ZK4800 core, the Jiujialu Formation is entirely absent, and the Permian Qixia Formation directly overlies the Cambrian Loushanguan Group. In most cores (CK33, CK69, ZK1712, ZK1720 and ZK1713), the thickness of Jiujialu Formation bauxites is modest, ranging from 8 to 25 m. Locally in the ZK1304, ZK5600 and ZK965 cores, the Jiujialu Formation shows much greater thicknesses, ranging from 80 to 110 m. The rapid thickness changes are a reflection of accumulation of Jiujialu Formation bauxites in sinkholes and dolines of the karstified Zunyi landscape. ZK5600 (i.e., the present study core) is especially suitable for analysis of the genesis of Jiujialu Formation bauxite deposits owing to its exceptional thickness (110 m) and its preservation of a larger number of bauxite-claystone cycles than seen in other cores regionally (Fig. 2).

4. Methods

The mineralogical compositions of the Jiujialu Formation bauxite samples were determined through a combination of petrographic examination of thin sections and X-ray diffraction (XRD). The XRD analysis was performed using a PANalytical X'Pert Pro model instrument in the State Key Laboratory of Geological Processes and Mineral Resources (GPMR), China University of Geosciences (Wuhan). The instrument has a Cu tube and a Ni filter and carries out a continuous scan with a speed of 8°/min at 40 kV and 40 mA. The mass percentages (mass%) of the main mineral phases were semi-quantified with an analytical error of ± 10%. A total of 42 samples were examined by XRD.

Scanning electronic microscopy (SEM) was used to investigate mineral morphology and microstructure. This analysis was performed using carbon-coated thin sections on a Hitachi SU8010 instrument equipped with an energy-dispersive X-ray spectroscopy (EDS) system in the State Key Laboratory of Biogeology and Environment Geology (BGEG), China University of Geosciences (Wuhan). Analytical conditions were 30 kV for the accelerating voltage and 5 nA for the beam current. EDS permitted the chemical composition of small (5-μm) analytical points to be determined.

Elemental analyses were carried out by ALS Chemex Laboratory (Guangzhou, China) on 97 whole-rock samples collected from drillcore ZK5600. Each whole-rock sample was crushed in a corundum jaw crusher (to 60 mesh) and then powdered in a tungsten carbide ring mill

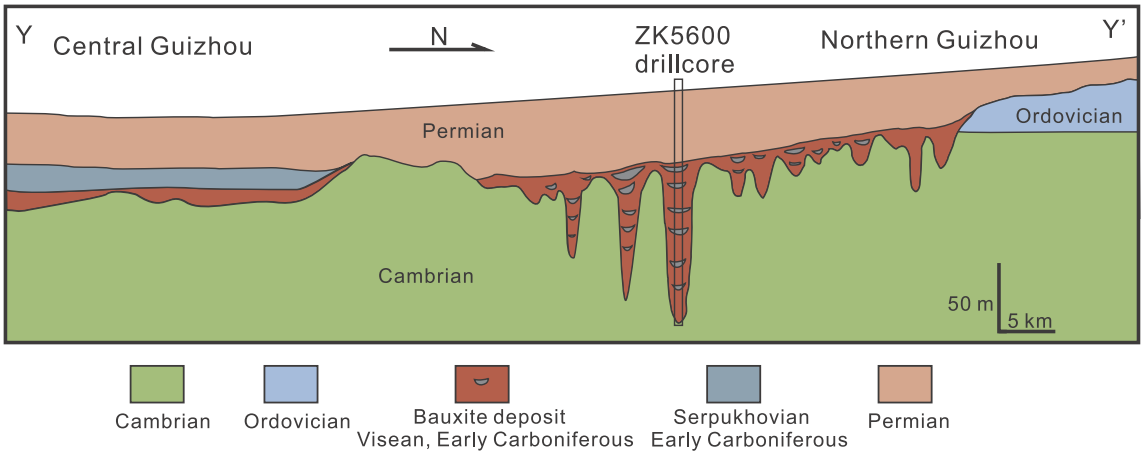

Fig. 2. Schematic sketch of structural relationships of the Jiujialu Formation and underlying/overlying strata in northern Guizhou to central Guizhou, based on the cross section Y-Y′ in Fig. 1B.

to finer than 200 mesh. Major-element measurements were made using a Shimadzu 1800X X-Ray fluorescence (XRF) unit with a detection limit of 0.1–1 ppm and an analytical precision better than ± 3% of reported values. Loss-on-ignition (LOI) was used to determine total volatile content. Trace element and rare earth element (REE) content was analyzed using an inductively coupled plasma-mass spectrometer (ICP-MS). Powdered samples were placed in Teflon bombs and moistened with a few drops of ultrapure water. Then, 1.5 ml HNO_3 and 1.5 ml HF were added to the sample powder. The sealed Teflon bombs were heated at 190 °C in an oven for 48 h. Then sample solutions were evaporated on a hot plate at ~115 °C to dryness. This was followed by adding 1 ml HNO_3 and evaporating to dryness a second time. The resultant salt was re-dissolved by adding ~3 ml of 30% HNO_3 and resealed and heated in the bomb at 190 °C for 24 h. The final solution was diluted with distilled water to ~100 mg prior to analysis. The detection limit for individual trace elements and REEs ranged from 2 to 8 ppm. All concentrations are given as weight percent (wt%).

Enrichment factors (EF), which reflect the enrichment or depletion of individual elements in a sample relative to a standard, were calculated as: $EF_X = (X/Ti)_{sample}/(X/Ti)_{standard}$, where X is the element of interest. EF_X values of > 1 and < 1 indicate enrichment and depletion, respectively, of element X. Because Al is mobile during the bauxitization process, Ti rather than Al was used for EF calculations (Tribovillard et al., 2006). Samples were normalized to post-Archean Australian shale (PAAS) (McLennan, 1989).

5. Results

5.1. Macro- and micromorphology

In vertical exposures, the bauxite ore in the ZK5600 core generally exhibits multiple layers, each consisting of an upper clastic sublayer (3–10 m) and a lower oolitic sublayer (0.5–5 m thick) (Fig. 3). The sublayers are internally homogenous in texture, and the transitions between the clastic and oolitic sublayers are generally sharp. However, areas of oolitic texture are occasionally observed above the contact between the clastic and oolitic sublayers (Fig. 4A), reflecting incomplete transformation of oolitic texture to clastic texture as the weathering process deepens the profile. The dark gray bauxitic claystone layers are located below the oolitic sublayers along a sharp contact. Most samples exhibit clastic (~50% of samples) and oolitic textures (~30% of samples), with rarer pelitomorphic textures (~20% of samples).

The clastic ore is white or light gray in color and composed of rounded to sub-angular grains ranging in size from 0.05 mm to 5 mm that are pervasively in contact, generating a grain-supported fabric. Individual clasts are composed of bright micron-sized diaspore crystals, and the clasts are embedded in a dark matrix with a fluidal-collomorphic texture, in which microcrystalline minerals (mostly Fe- and Al-oxides) are rhythmically arranged (Bárdossy, 1982) (Fig. 4B). Clastic grains and matrix in the bauxite ore layers have similar mineralogical compositions, but the matrix has a higher Fe-oxide content (20–30%) than the clasts (10–15%) (Fig. C). Grains in the clastic bauxite ore layers have laminar, concentric outer coatings (=ooids or spheroids) consisting of red (Fe-oxide) or white (Al-oxide) materials (Fig. 4D–F).

The oolitic ore consists of elliptical or spherical ooids ranging in diameter from 0.02 mm to 2 mm and showing grain support. All ooids exhibit concentric fabrics with alternating bright (Al-oxide) and dark (Fe-oxide) laminae. Most ooids are whole, reflecting an authigenic origin, but internal and marginal crystallographic patterns in some broken ooids indicate that partial dissolution and remineralization of ooids were common processes during the weathering process (Fig. 4G, H). Some ooids also contain radial micron-sized shrinkage fractures (Fig. 4D).

Pelitomorphic textures (i.e., homogeneous and massive, without macroscopic bedding or clasts) are characteristic of dark gray bauxitic claystone. These samples consist mainly of microcrystalline clay minerals (e.g., illite, kaolinite) and less abundant Al-oxides (diaspore) (Fig. 4I and J). Diagenetic pyrite is common in these layers, with individual euhedral crystals varying from micron-sized to centimeter-

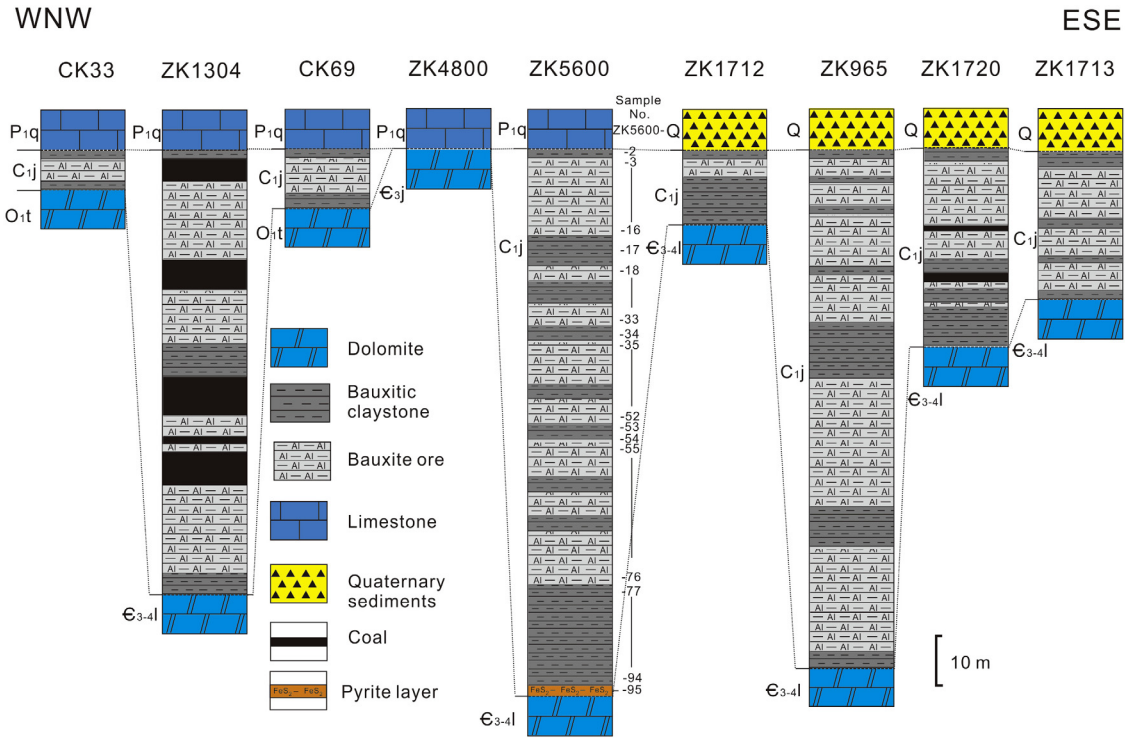

Fig. 3. Lithologic columns for the Lower Carboniferous Jiujialu Formation bauxite deposit in the Zunyi area, northern Guizhou. Locations of drillcores are shown in Fig. 1C–D. Sampling sites in drillcore ZK5600 are marked on the right side of the column.

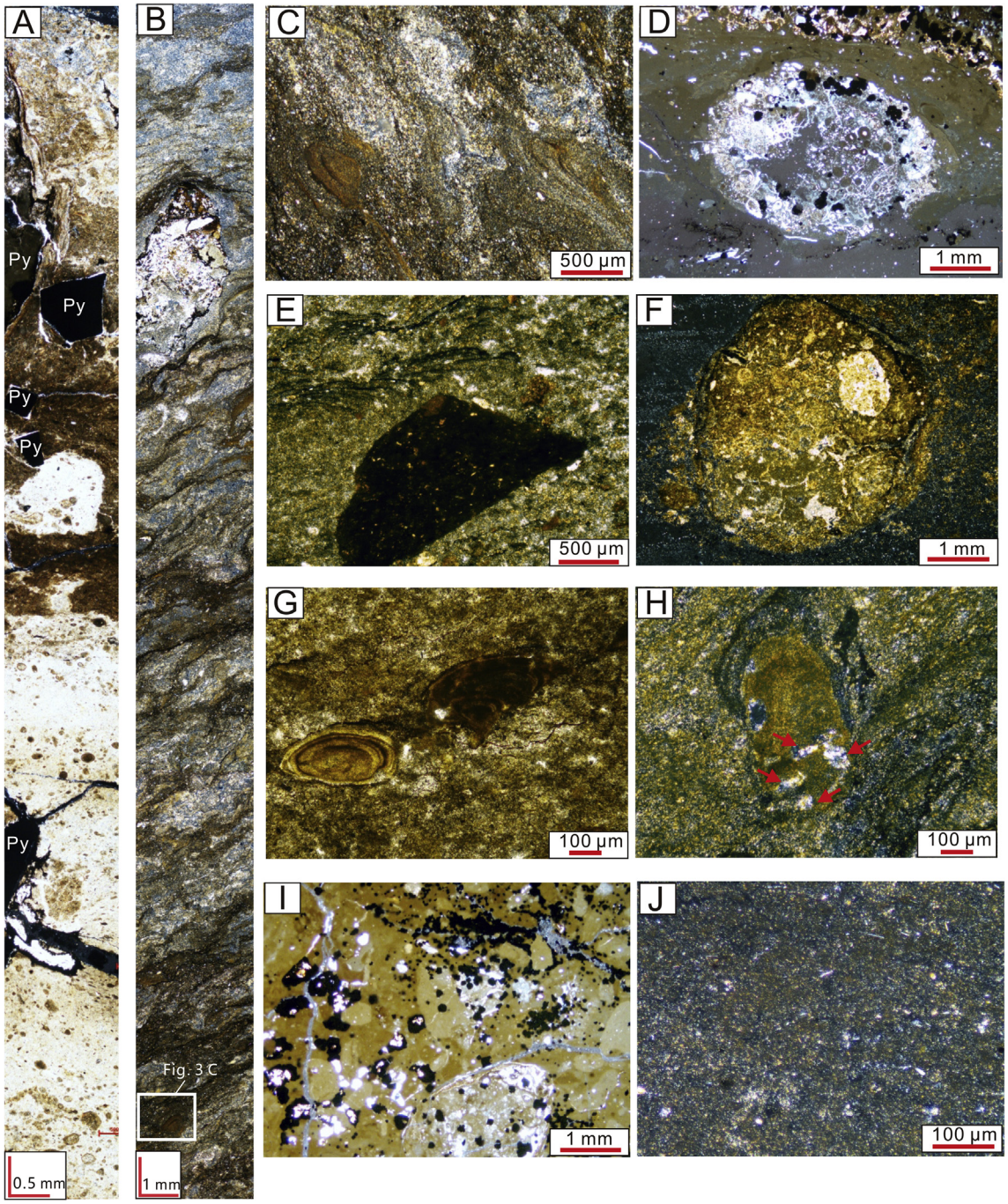

Fig. 4. Thin-section photos for samples (A) Clastic and oolitic textures in sample ZK5600-29; (B) Clastic texture in sample ZK5600-28; (C) Contact relationship between clastic grains and matrix in sample ZK5600-28; (D) Bauxite clast with internal oolitic texture in sample ZK5600-18; (E) Bauxite clasts in sample ZK5600-11; (F) Bauxite clasts in sample ZK5600-20; (G) Aluminum-oxide oolite in sample ZK 5600-26; (H) Oolite partially replaced by illite in sample ZK5600-88 (red arrow); (I) Massive texture in bauxitic claystone sample ZK5600-17, black clusters are pyrite; (J) Massive texture in bauxitic claystone sample ZK5600-22. Py – pyrite. (For interpretation of the references to color in this figure legend, the reader is referred to the web version of this article.)

sized.

5.2. Mineralogy

XRD analysis indicates that the main minerals in the 27 bauxite ore samples are diaspore (65–95%, avg. 84%), illite (0–35%, avg. 19%), and pyrite (up to 18% in samples ZK5600-48 and ZK5600-35 but 0–3% in most samples) (Fig. 4A and B). In SEM images, diaspore crystals have a columnar shape with lengths of 0.2–0.5 μm and are present mainly embedded in lamellar illite grains (Fig. 5A).

The bauxitic claystone layers in ZK5600 mostly have massive and homogeneous textures. Most samples (n = 14) are composed of illite (15–94%, avg. = 55%) and diaspore (18–65%, avg. = 40%). The lower bauxitic claystone layers contain relatively large amounts of pyrite (3–35%, avg. = 22%; in ZK5600-94 to ZK5600-78) and smaller amounts of kaolinite (2–3%, avg. = 2%; in ZK5600-94 to ZK5600-86 and ZK5600-66) (Fig. 4C), but pyrite disappears in the middle and upper parts of the deposit. A single sample from the base of the drillcore (ZK5600-96) is pyrite-dominated (90% pyrite) and also contains small amounts of the rare earth mineral churchite [(Y, Nd, Er, Dy)PO_4 –

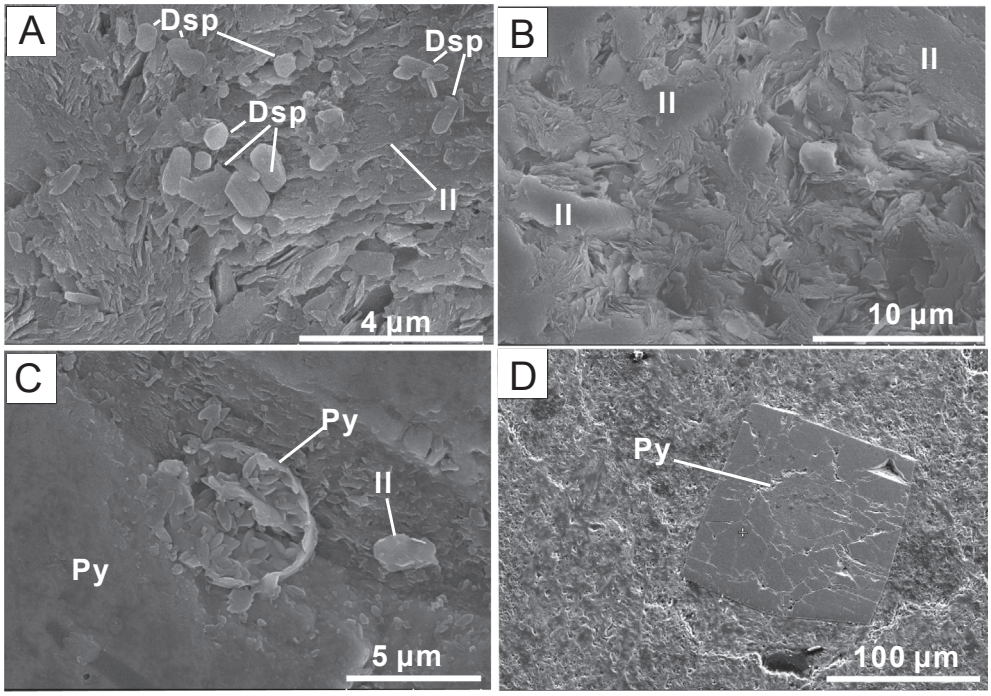

Fig. 5. SEM images for (A) Intersection relationship of diaspore and illite in sample ZK5600-20; (B) Illite matrix in sample ZK5600-88; (C) Bacterial structures, pyrite, and detrital illite in ZK5600-20; (D) Automorphic pyrite in sample ZK5600-26. Dsp-diaspore; II-illite; Py-pyrite.

$2H_2O$, 10%] (Fig. 4D). In SEM images, the diaspore crystals are columnar, short-columnar, or spherical in shape with lengths of 1–5 μm (Fig. 5A). Illite grains form most of the matrix of the bauxitic claystone samples of the Zunyi deposit. The abundance of illite within the bauxite deposit is uncommon, as detrital illite is usually concentrated at the base of bauxite profiles (Bárdossy, 1982). At Zunyi, lamellar illite encases many diaspore crystals, indicating formation or translocation after diaspore growth (Fig. 5A–C). In some samples, illite replaces the original minerals, indicating a diagenetic origin through potassium metasomatism (Fig. 3H). Two types of pyrite can be found in the study samples, including 1) pyrite framboids with grain sizes of 5–10 μm (Fig. 5C), and 2) euhedral pyrite with grain sizes of 100 μm to 2 cm (Fig. 5D).

5.3. Major elements

All bauxite ore samples contain Al_2O_3 > 55% (n.b., 55% is the limit of Chinese standard value for bauxite industrial grade), ranging from 55.6% to 77.7% with an average of 70.0%, and the average EF_{Al} of the bauxite ore samples is 1.25 (n = 65). EF_{Al} > 1 indicates that Al was enriched in bauxite ore samples during the bauxitization process. As another resistate element, TiO_2 in the bauxite ore samples ranges from 1.6% to 4.2% with a mean of 3.0%. Bauxite ore samples contain low SiO_2 (1.4–27.7% with a mean of 10.6%), low Fe_2O_3 (0.45–18.7% with a mean of 1.9), and low alkali and alkaline earth elements (except K_2O), e.g., CaO (mean 0.06%, max. 0.29%), Na_2O (mean 0.22%, max. 0.25%), and MgO (mean 0.22%, max. 0.25%). Some samples contain high K_2O, and K_2O varies greatly overall (0.30–5.9% with a mean of 2.0%). Except for Al and Ti, all other major elements in the bauxite ore samples show strong depletions based on enrichment factors, e.g., mean EF_{Si} = 0.05 and mean EF_{Fe} = 0.10. The Al_2O_3/SiO_2 ratio of the bauxite ore samples ranges from 4.0 to 46.5 with a mean of 12.0, indicating the high quality of the bauxite ore samples.

The bauxitic claystone samples contain Al_2O_3 < 55% (19.0–54.0% with a mean of 38.4%), but Al in the bauxitic claystones was also enriched during the bauxitization process (average EF_{Al} = 1.22, n = 31). Their TiO_2 content is lower than that of the bauxite ore (0.7–3.1% with a mean of 1.7%). The SiO_2 (2.1–46.6% with a mean of 26.9%) and Fe_2O_3 contents (0.56–35.5% with a mean of 12.4%) are higher than in the bauxite ore. CaO (mean 0.16%, max. 0.42%), Na_2O (mean 0.22%, max. 0.16%), and MgO (mean 0.67%, max. 1.4%) are also low in the bauxitic claystone samples. However, the K_2O contents are generally high (0.47–9.8% with a mean of 5.7%), and EF_K shows enrichments of potassium in 14 out of 31 bauxitic claystone samples.

As the potential parent material for the Jiujialu Formation bauxite deposit, shales of the Lower Ordovician Meitan and Tongzi formations were collected and analyzed. The bauxite deposit, the Ordovician shales, and modern laterites in central Guizhou together show a strong negative correlation between SiO_2 and Al_2O_3 ($r = -0.85$; $p(\alpha) < 0.01$; n = 103; Fig. 6A), indicating major loss of silicon during the chemical evolution of the bauxite deposits. No significant correlations were found in Fe_2O_3-Al_2O_3 and CaO-Al_2O_3 crossplots (Fig. 6B and C), but two clusters are apparent: (1) bauxite ore samples with high Al_2O_3, low Fe_2O_3, and low CaO contents, and (2) bauxitic claystone samples with lower Al_2O_3, higher Fe_2O_3, and higher CaO contents. For the bauxite ore samples, a strong negative correlation is observed between K_2O and Al_2O_3 ($r = -0.74$; $p(\alpha) < 0.01$; n = 65), but the Ordovician shales and bauxitic claystone samples show a positive K_2O-Al_2O_3 trend with peak values at K_2O = 9.8% and Al_2O_3 = 34.1% (ZK5600-94) (Fig. 6D). A strong positive correlation also exists between TiO_2 and Al_2O_3 ($r = +0.93$; $p(\alpha) < 0.01$; n = 103; Fig. 6E), reflecting the immobility of Ti during chemical weathering.

5.4. Trace and rare earth elements

In the 63 bauxite ore samples, most trace elements show strong or moderate depletion relative to PAAS, including Ba (EF = 0.01–0.2, $EF_{avg.}$ = 0.05), Co (EF = 0.01–1.0, $EF_{avg.}$ = 0.04), Cr (EF = 0.3–0.9, $EF_{avg.}$ = 0.5), Ni (EF = 0.01–0.4, $EF_{avg.}$ = 0.07), Sr (EF = 0.03–1.4, $EF_{avg.}$ = 0.2), Y (EF = 0.3–0.9, $EF_{avg.}$ = 0.45), and Nd (EF = 0.06–2.5, $EF_{avg.}$ = 0.4). Some elements show variable depletions and enrichments, yielding average values close to or higher than PAAS, including Sc (EF = 0.5–2.3, $EF_{avg.}$ = 1.1), Ga (EF = 0.4–1.2, $EF_{avg.}$ = 0.7), Th (EF = 0.9–2.6, $EF_{avg.}$ = 1.25), and Zr (EF = 0.6–3.0, $EF_{avg.}$ = 0.9).

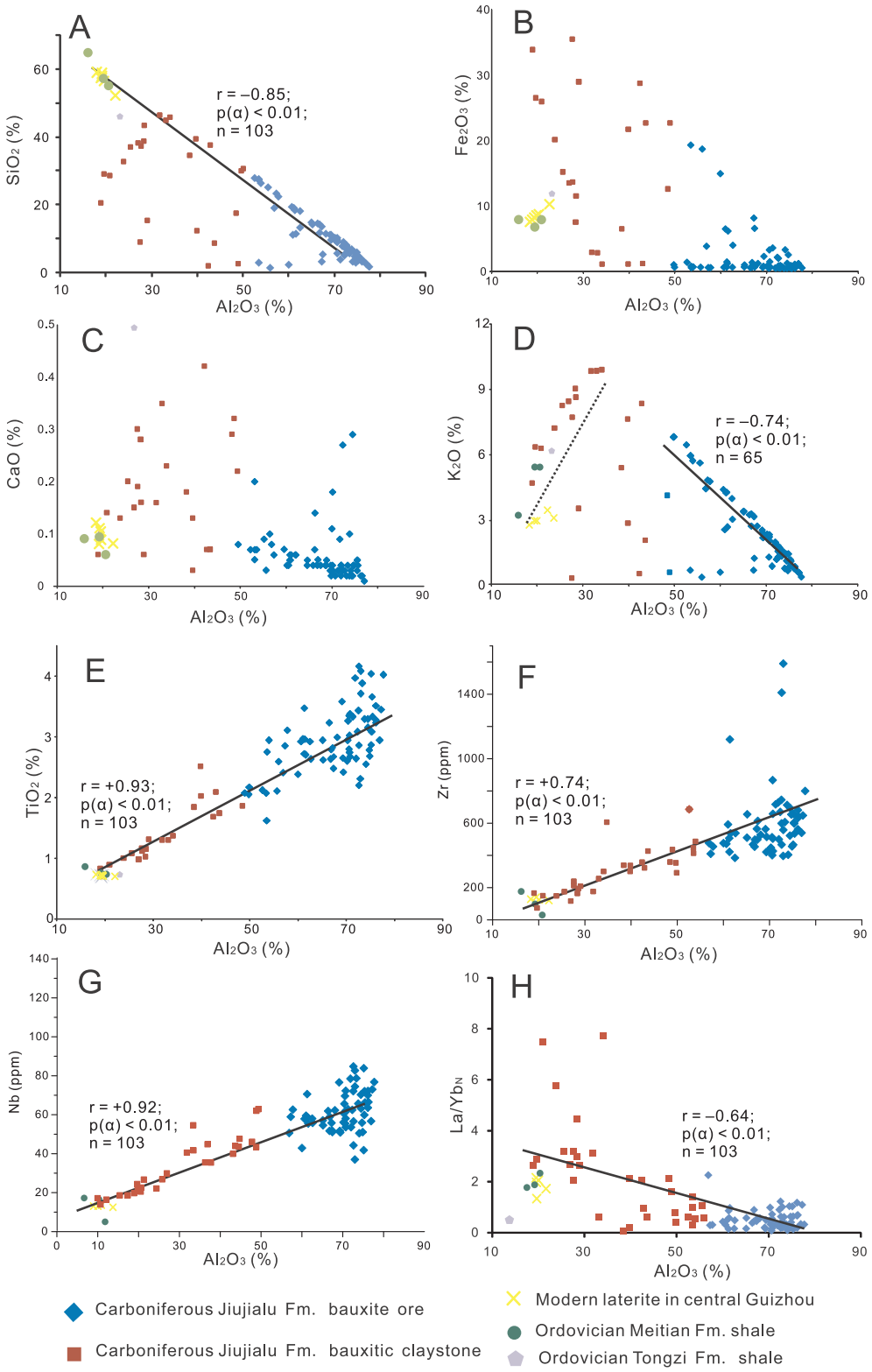

Fig. 6. Al_2O_3 versus (A) SiO_2, (B) Fe_2O_3; (C) CaO; (D) K_2O; (E) TiO_2, (F) Zr, (G) Nb, and (H) La_N/Yb_N in the Lower Carboniferous Jiujialu Formation bauxite deposit, Ordovician shale, and modern laterite in central Guizhou. Ordovician shale and modern laterite samples are from Cao et al. (2012).

In the 31 bauxitic claystone samples, trace elements commonly show enrichments relative to PAAS, including Sc (EF = 0.8–7.0, $EF_{avg.}$ = 1.85), Ga (EF = 0.3–1.0, $EF_{avg.}$ = 1.4), Th (EF = 1.0–2.3, $EF_{avg.}$ = 1.5). Some trace elements show overall enrichments but highly variable concentrations between claystone layers, such as Nd (EF = 0.07–11.8, $EF_{avg.}$ = 1.5), Y (EF = 0.19–10.4, $EF_{avg.}$ = 0.85) and Ni (EF = 0.05–3.1, $EF_{avg.}$ = 0.5). The strong enrichments in individual layers are linked to the vertical mobility or translocation of these trace elements with the weathering profile (Mongelli et al., 2014). Zr (EF = 0.6–1.5, $EF_{avg.}$ = 0.85) show slight depletions on average, with concentrations similar to those in the bauxite ore. Certain trace elements show strong depletions: Ba (EF = 0.02–0.5, $EF_{avg.}$ = 0.2), Co

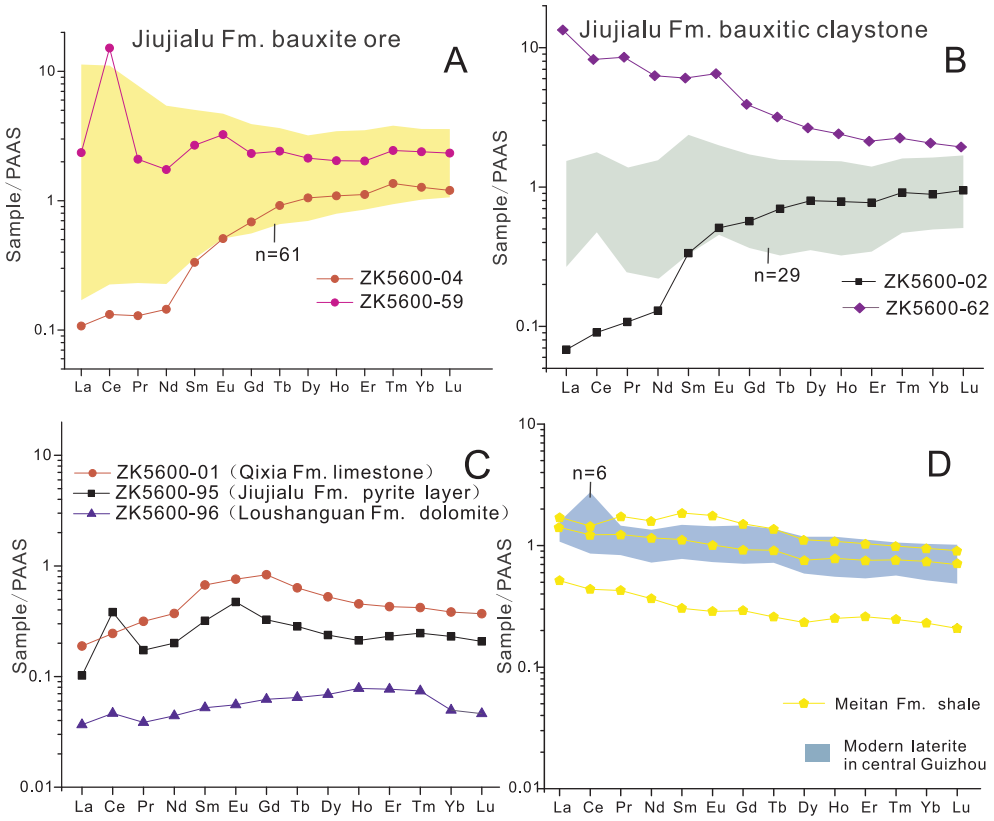

Fig. 7. PAAS-normalized REE distributions. (A) Bauxite ore and (B) bauxitic claystone samples in the Lower Carboniferous Jiujialu Formation from drillcore ZK5600; (C) Lower Permian Qixia Formation limestone, Upper Cambrian dolostone, and Lower Carboniferous Jiujialu Formation pyrite from drillcore ZK5600; (D) Lower Ordovician Meitan Formation shale and modern laterite in central Guizhou. All samples normalized to post-Archean Australian shale (PAAS) (McLennan, 1989).

(EF = 0.01–0.5, $EF_{avg.}$ = 0.3), and Sr (EF = 0.03–1.4, $EF_{avg.}$ = 0.2). Strong positive correlations are shown by Zr and Al_2O_3 ($r = +0.74$, $p(\alpha) < 0.01$; $n = 103$) and by Nb and Al_2O_3 ($r = +0.92$; $p(\alpha) < 0.01$; $n = 103$), reflecting the resistate character of these trace elements (Boski and Herbosch, 1990; Mongelli, 1993) (Fig. 6F and G).

The ΣREE of the bauxite ore samples ranges from 31 to 1736 ppm, with a mean of 338 ppm. These samples display uniform heavy REE (HREE) but varying light REE (LREE) concentrations, with La_N/Yb_N ratios ranging from 0.08 to 7.7 (mean = 0.90). This pattern reflects the greater stability of HREEs during the weathering process, whereas LREEs are more easily mobilized (Braun et al., 1993). Positive Ce anomalies are also seen in most bauxite ore samples (0.97–6.8 with a mean of 1.7). On the other hand, most bauxitic claystone samples show flat (i.e., lithogenous) REE patterns, although samples ZK5600-02, -53, -62, and -88 show either LREE-enriched or HREE-enriched patterns (Fig. 7B). Both positive and negative Ce anomalies are seen in the bauxitic claystone samples (0.5–2.5 with a mean of 1.3). For bauxite ore and bauxitic claystone samples, Eu anomalies (Eu/Eu^*) range from 0.8 to 1.4 with an average of 1.0.

6. Discussion

6.1. Evidence for in situ weathering origin of bauxite ore

Weathering profiles usually preserve characteristic structures and textures due to leaching and remineralization processes (Bárdossy, 1982; Valeton, 1999). In a typical weathering profile, leaching will lead to development of vertical fractures along which vadose soil water flows, thus breaking the weathered materials into clasts. When Fe-oxides and Al-oxides later precipitate in these fractures, the clasts are then surrounded by matrix, generating a clastic texture (also called "pseudo-breccia") (Bárdossy, 1982; Boulangé and Carvalho, 1997; Lucas, 1997). The leaching process results in vertical translocation of elements within the weathering profile, and Al and Fe can be transported colloidally under suitable conditions and then precipitate as chemical ooids (also called "spheroids", "pisoids", or "nodules") deeper in the soil profile. This process thus leads to formation of bauxite deposits with a clastic layer overlying an oolitic layer (Bárdossy, 1982; Liao and Liang, 1991).

Both macroscopic and micromorphologic observations show evidence of an *in situ* weathering origin, rather than a redeposition origin, for bauxite ore layers in ZK5600. First, the presence of both clastic and oolitic bauxite sub-layers (Fig. 4A) is a typical feature of *in situ* weathering profiles (Bárdossy, 1982; Boulangé and Carvalho, 1997; Lucas, 1997). Second, fracturing of clasts or ooids does not reflect mechanical breakage in transport but, rather, *in situ* breakage and fracture fills (Fig. 4B) (Bárdossy, 1982; Liao and Liang, 1991). Third, the clastic grains and matrix in the bauxite ore layers have similar mineralogical compositions (Fig. 4C), showing that they formed via the same weathering process (Bárdossy, 1982; Liao and Liang, 1991). However, the matrix has a higher Fe-oxide content than the clasts (Fig. 4A–C), reflecting the higher mobility of Fe during the weathering process (Bárdossy, 1982; D'Argenio and Mindszenty, 1995).

6.2. Parent rock affinity

Earlier studies have inferred that the parent rock of the Jiujialu Formation bauxite deposits consisted of both shales of the Lower Ordovician Meitan and Tongzi formations and dolostones of the Cambrian Loushanguan Group (Ling et al., 2017; Liu, 1991). Based on calculations of Al enrichment efficiency, elemental ratios, and REE patterns, we infer that the Ordovician shales must have been the main source materials for the bauxite deposits of the Zunyi area.

(1) Weathering of pure limestone or dolostone usually fails to provide enough aluminum for bauxite deposit formation (Bárdossy, 1982), i.e., the thickness of the carbonate unit needed to generate the Al_2O_3 content of bauxite usually exceeds the actual thickness of *in situ* carbonate deposits. At Zunyi, the Al_2O_3 content of the underlying Cambrian Loushanguan Group ranges from 0.15 to 0.25%

(Cao et al., 2012, and this study). At this concentration, at least 1000 m of Loushanguan Group dolostone would have to dissolve to form a 5-m-thick bauxite deposit containing 50% Al_2O_3. However, the total thickness of carbonates in the Zunyi area was only 600–900 m (Weng et al., 2011), which is insufficient to generate bauxite deposits from 8 to 110 m in thickness. Thus, it seems unlikely that the main parent rocks of the Zunyi bauxite were Loushanguan Group dolostones.

(2) As resistate elements are largely retained in soils during chemical weathering, their ratios provide a geochemical signature that can be compared with elemental ratios in potential parent rocks. The shales of the Lower Ordovician Meitan and Tongzi formations and the bauxite deposits of the Jiujialu Formation exhibit nearly identical ratios between Al_2O_3 and other resistate elements (e.g., Ti, Zr and Nb; Fig. 6E–G), which is consistent with (but does not prove that) the bauxites were derived through weathering of these shales. The bauxites and shales show a strong negative correlation between Al_2O_3 and SiO_2 (Fig. 6A), which reflects losses of Si during weathering of the shale (SiO_2 > 55%) into bauxite ore (SiO_2 < 30%). These trace-element patterns thus show a geochemical affinity of Lower Ordovician Meitan and Tongzi formation shales with Jiujialu Formation bauxites.

(3) REE distributions provide another type of geochemical fingerprint that can be used to evaluate potential sources of bauxite (Braun et al., 1993). The Cambrian Loushanguan Group dolostones show low ΣREE contents and HREE-enriched patterns (Fig. 7C), which are different from the Zunyi bauxite deposit. On the other hand, the Ordovician Meitan Formation shales show high ΣREE contents and flat REE patterns (Fig. 7D), features that are similar to the Jiujialu Formation bauxitic claystones (Fig. 7B). Eu anomalies (Eu/Eu^*, avg. 1.04) in samples of the bauxite deposit are similar to Eu/Eu^* values of the underlying Ordovician shales (0.96–1.15, avg. = 1.06, n = 5). Since Eu anomalies in a weathering profile are mostly inherited from the parent rock (Mongelli 1993; Wang et al., 2010), the similar Eu anomalies in the bauxite deposit and underlying shales indicate their affinity.

6.3. Multistage formation of the Lower Carboniferous Jiujialu Formation bauxite deposit

The 110 m thickness of bauxitic sediment in drillcore ZK5600 at Zunyi represents long-term filling of a sinkhole or doline, and the regular alternation of bauxite ore and bauxitic claystone layers records changes in the intensity of chemical weathering and leaching that can be attributed to paleoclimatic and hydrologic changes during bauxite formation. Petrologic, mineralogical, and geochemical data reveal the presence of seven cycles in the ZK5600 core, and each cycle can be regarded as a weathering profile. The cycles range from 8 m (thinnest; Cycle II) to 33 m (thickest; Cycle I), with the other cycles between 10 and 25 m in thickness. Each cycle has a lower layer composed of dark-gray massive bauxitic claystone layer, characterized by low Al_2O_3 and TiO_2, high SiO_2 and K_2O, and illite as the dominant mineral component, and an upper layer composed of light-gray or white clastic bauxite ore, characterized by high Al_2O_3 and TiO_2, low SiO_2 and K_2O, and diaspore as the main mineral component. During the bauxitization process, resistate elements (e.g., Al and Ti) accumulated as a residuum, while mobile elements (e.g., Si, alkali elements, and alkali earth elements) were leached out of the soil (Bárdossy and Combes, 1999; Liu et al., 2010; Mongelli et al., 2015; Wang et al., 2011; Zarasvandi et al., 2010). REEs were also influenced by weathering, as shown by a strong negative correlation between La_N/Yb_N and Al_2O_3 ($r = -0.64$; $p(\alpha) < 0.01$; n = 103), reflecting increasing losses of LREEs (except for Ce) concurrently with concentration of Al as weathering proceeded (Fig. 6H). The bauxite ore layers thus reflect a higher degree of chemical weathering than the bauxitic claystone layers.

The chemical index of alteration (CIA; Nesbitt and Young, 1982) and chemical index of weathering (CIW; Harnois, 1988) were used in this study to reconstruct changes in chemical weathering intensity and element mobility during formation of the Jiujialu Formation bauxite deposits in the Zunyi area. High CIW values (99–100) for the bauxite ore and bauxitic claystone samples indicate intense chemical weathering. However, the bauxite ore and bauxitic claystone show distinctively different CIA values, with higher values (91–99, avg. 96) in the ore samples and lower values (74–99, avg. 85) in the claystone samples. These values show that the bauxite ore formed through more intense chemical weathering and leaching than the bauxitic claystone samples (Nesbitt and Markovics, 1997). CIA exhibits an overall stratigraphic pattern as well. The lower part of Cycle I is characterized by relatively low values (~75; from 589.7 m to 577.4 m), reflecting moderate weathering intensity during the initial period bauxite formation. Above 577.4 m, CIA increased abruptly to values mostly > 90, reflecting intensified chemical weathering beginning in the middle of Cycle I. Through the remainder of the whole bauxite deposit, the CIA profile shows six declines, each corresponding to a bauxitic claystone layer and an increase in illite content. These layers represent phreatic-type bauxite deposits formed in a water-logged environment under conditions of less intense chemical weathering (Fig. 8A, B). The bauxitic claystone samples exhibit a strong positive correlation of CIA with Ce/Ce^* ($r = +0.73$, $p(\alpha) < 0.05$, n = 31) and a negative correlation with La_N/Yb_N ($r = -0.39$, $p(\alpha) < 0.05$, n = 31), implying that the mobility of REEs was also controlled by the weathering process.

In an A-CN-K diagram, samples of the Zunyi bauxite deposit, Ordovician shale, and modern laterite plot along a line parallel to the A-K axis that is distinctly non-colinear with the UCC-PAAS weathering trend line (Fig. 9; Nesbitt and Young, 1984). The usual explanation for trends parallel to the A-K axis is potassium metasomatism of sedimentary rocks and paleosols (Fedo et al., 1995). However, the Ordovician shales, which are the main parent rock of the bauxite deposits, are characterized by high K_2O content (5–10%) and, thus, are the most likely source of potassium (BGMRGZP, 1987; Yin and Chen, 2007). This inference also accounts for the unusually high illite content of the bauxite deposit. K-rich muscovite and K-feldspar in the Ordovician shales first transformed to illite during moderately intense weathering, as characterizes the bauxitic claystone layers, and then transformed to kaolinite under conditions of intense chemical weathering, but with some residual illite preserved even in the bauxite ore (Bárdossy, 1982). During diagenesis, the Ordovician shales provided K-rich fluids that influenced the formation of secondary illite (Berger et al., 1999; Elliott and Haynes, 2002), and that may have been the main K source for the potassium metasomatism trend in the A-CN-K diagram (Fig. 9).

We undertook mass balance calculations to quantify changes in major- and trace-element compositions of the host rock during formation of the Jiujialu Formation bauxite deposit. The average chemical composition of the Ordovician shale samples was used as the starting point for mass balance calculations, with Ti chosen as the monitor element (MacLean, 1990; MacLean and Barrett, 1993; Young and Nesbitt, 1998). From the mass balance results (Fig. 8B), it can be seen that Al in the lower part of the core (Cycles I, II and III) was stable around zero, reflecting limited mobility during bauxite formation, although some positive values (i.e., Al enrichment) are present at the tops of Cycles I and III. Higher in the profile, the bauxite ore layers show Al losses in Cycle IV, variable enrichment or depletion in Cycle V, and Al losses again in Cycles VI and VII. In the bauxitic claystone layers of Cycle IV-VII, Al losses (−4% to −3%) exceed those of the adjacent bauxite ore layers (−3.5% to −1%). Al losses are accompanied by TiO_2 increases, rising from +2% in the lower part of the profile to +4% in its upper part (Fig. 8A). These observations likely reflect greater weathering intensity in the upper part of the Zunyi profile. Maximum Al enrichment is usually seen in the upper part of each cycle, which is linked with intense chemical weathering at the top of each weathering profile. Si, K, Na and Mg show similar patterns of losses and gains within the study core, with relatively stable losses in the bauxite ore

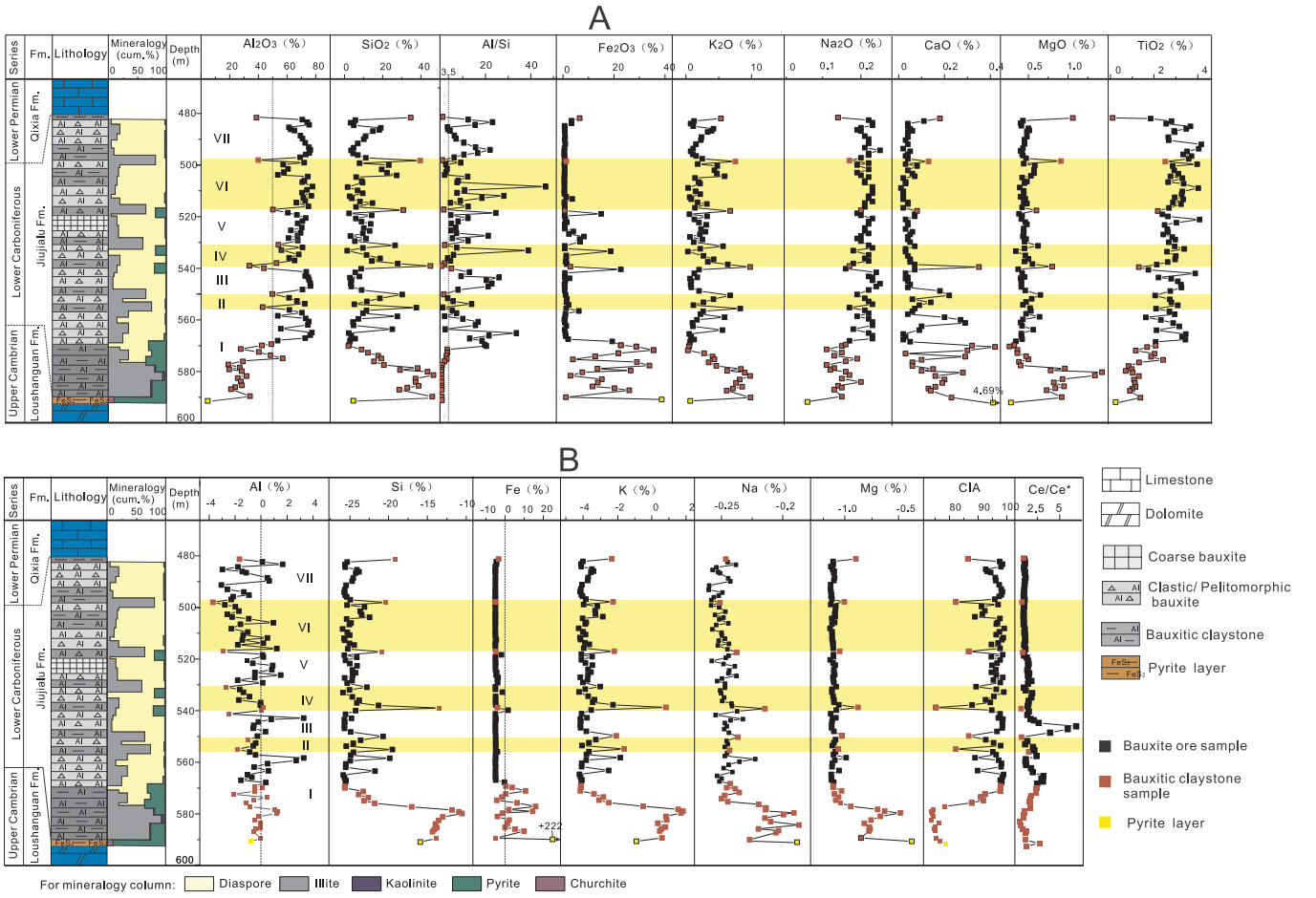

Fig. 8. (A) Integrated column of petrology, mineralogy, and geochemistry, and (B) mass balance calculation results for some major elements in drillcore ZK5600.

layers (Si: −25% to −23%, K: −4% to −3%, Na: about −0.25%; Mg: about −1%), although K shows local enrichments in the bauxitic claystone layers (Si: −25% to −10%, K: −4% to +2%, Na: about −0.23%; Mg: about −1%). Fe shows both losses and enrichments in the lower part of Cycle I but stabilizes at −5% in the remainder of the profile. As to rare elements in the bauxite deposit, some high field-strength elements (HFSE) show relatively small losses (e.g., Zr: −57% to −18%, avg. = −41%; Hf: −1.3% to −0.03%, avg. = −0.65%) or gains (Nb: +0.07% to +4.7%, avg. = +3.4%; Ta: +0.02% to +0.48%, avg. = +0.09%), indicating stability of these elements during the weathering process. Losses of certain elements may have been linked to losses of heavy minerals (e.g., zircon) during transport of initial weathering products from the surface into the karstic depression. Certain other elements, e.g., REEs and yttrium (Y), show strong variation between losses and gains through the whole profile (e.g., La: −45% to +180%, Yb: −0.9% to +13%, Y: −14% to +203%), indicating strong mobility of these elements during the bauxitization process.

6.4. Mechanism for multistage formation of bauxite deposits

As is typical of Kazakhstan-subtype bauxite deposits, the Jiujialu Formation bauxite formed through intense karstification of a suitable bedrock type under specific paleoclimate conditions. Tectonic uplift and long-term landscape exposure at Zunyi (from the late Ordovician to the early Carboniferous) established the geomorphological boundary conditions for bauxitization (Bárdossy and Combes, 1999; D'Argenio and Mindszenty, 1995; Deng et al., 2010). During the Carboniferous, the South China Craton was located near the paleo-equator (Zhu et al., 1998), and its paleoclimate was controlled by the Intertropical Convergence Zone (ITCZ). High mean annual temperatures (MAT) and strong precipitation associated with the ITCZ provided appropriate climate conditions for bauxite formation (Price et al., 1997; Yu et al., 2018). Intense chemical weathering under warm and humid conditions is indicated by the high CIA values (> 90) and diaspore-dominated mineral composition of the Zunyi bauxite ore (Nesbitt and Young, 1984; Trolard and Tardy, 1987).

Groundwater table (GWT) fluctuations were probably responsible for horizonation in the Zunyi bauxite deposit. Low GWT elevations resulted in better drainage of soil water and more oxidizing conditions, favoring bauxite formation, whereas high GWT elevations resulted in water-logged soils and more reducing conditions, favoring development of bauxitic claystone (or coal) deposits. Ce anomalies can be a reliable indicator of redox conditions in a weathering profile (Mongelli, 1993; Mongelli, 1997; Wang et al., 2013a). Under oxic conditions, Ce is oxidized to Ce(IV) and mobilized, leading to Ce enrichment and a positive Ce anomaly in some layers (accumulating as Ce-bearing minerals; Wang et al., 2010), but Ce depletion and a negative Ce anomaly in others (Braun et al., 1990). In contrast, under suboxic or anoxic conditions, Ce (III) is not fractionated relative to other REEs and no anomaly is produced. Low GWTs result in vadose-type bauxite deposits consisting of light-gray or white clastic bauxite ore layers that form under oxic conditions, favoring diaspore growth and positive Ce anomalies (Fig. 8) (D'Argenio and Mindszenty, 1995). In contrast, high GWTs result in phreatic-type bauxite deposits that are dark-colored, illite- and pyrite-rich, have negative Ce anomalies, and are associated with coals (Fig. 8). Coal deposits are generally related to stagnant soil waters, usually in swamp environments in which the ground surface may be shallowly

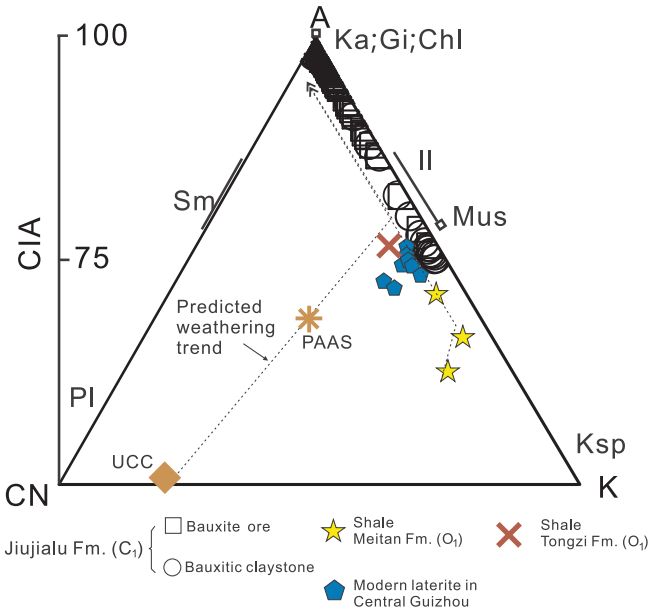

Fig. 9. A-CN-K diagram for the Jiujialu Formation bauxite deposits, Ordovician shales, and central Guizhou modern laterites. The predicted weathering trend line is constrained by Upper Continental Crust (UCC) and post-Archean Australian shale (PAAS) compositions. Ordovician shale and modern laterite samples are from Cao et al. (2012), UCC data are from Rudnick and Gao (2003), PAAS data are from McLennan (1989). A = Al_2O_3, CN = $CaO^* + Na_2O$, K = K_2O, all oxides are in molar proportions (mol %), CaO^* represents Ca in silicate-bearing minerals only. Ka = kaolinite; Gi = gibbsite; Chl = chlorite; Sm = smectite; Il = illite; Pl = plagioclase; Ksp = K-feldspar.

submerged (Kalaitzidis et al., 2010; Moore, 1989). In drillcore ZK1304 of the Zunyi area, pyrite-rich coal layers within the Jiujialu Formation bauxite deposit were inferred to be evidence of a high groundwater table and stagnant soil waters (Bárdossy, 1982; Liu et al., 2016). In drillcore ZK5600 (i.e., the present study core), the dark-gray massive bauxitic claystone layers formed during intervals of high GWTs (D'Argenio and Mindszenty, 1995).

Groundwater table fluctuations during formation of the Lower Carboniferous bauxite deposits at Zunyi were probably driven by glacio-eustatic cycles of the LPIA. During the Carboniferous, continental glacial deposits were widespread in Gondwana (Fielding et al., 2008; Montañez, 2016), and the Visean was an interval of rapidly expanding continental ice mass (Caputo et al., 2008; Montañez, 2016; Liu et al., 2018), characterized by increasingly large eustatic fluctuations (Rygel et al., 2008). Although located at low latitudes, the South China Craton experienced far-field effects of these glacial events. Positive carbon isotope excursions and exposed surfaces in Visean marine carbonate sequences of South China are consistent with a major eustatic fall (Liu et al., 2015; Qie et al., 2011; Wang et al., 2013b). The Zunyi area was located on the coastal karst plain of the South China Craton during the early Visean (Fig. 1B), and eustatic fluctuations would have directly changed GWT elevations in this area (Nicholls and Cazenave, 2010; Rotzoll and Fletcher, 2012).

The lithologic succession of the ZK5600 core reveals at least six eustatic cycles with magnitudes of > 20 m during the Visean. Formation of the bauxite deposits at Zunyi can be summarized as follows: 1) During their initial formation, ferralitic weathering products accumulated in shallow sinkholes and dolines of the karstified surface of underlying Cambrian and Ordovician formations (Fig. 10A). 2) The depth of karst depressions increased along fracture zones, especially during low GWT intervals when downward flow of soil waters and chemical leaching was strongest (Fig. 10B). 3) During high GWT intervals, submergence of sinkholes and dolines resulted in development

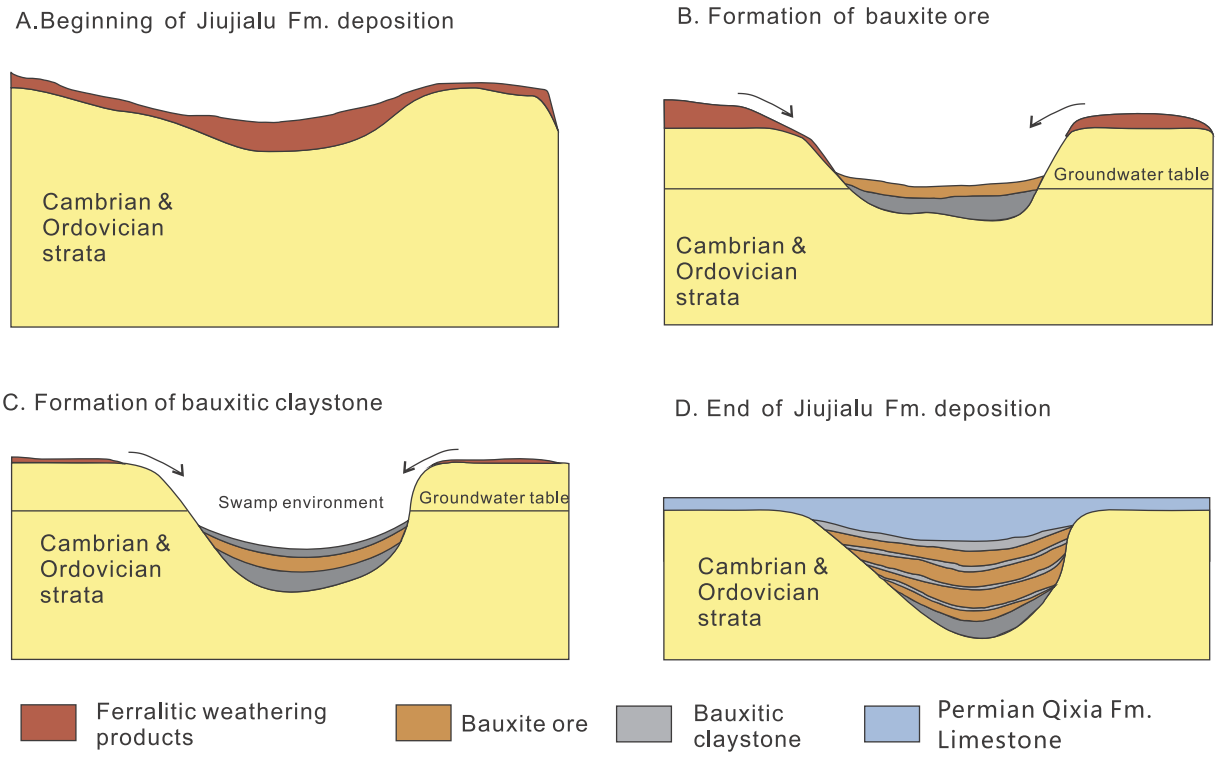

Fig. 10. Formation process of the Lower Carboniferous Jiujialu Formation bauxite deposits in the Zunyi area, Guizhou. (A) During the initiation stage of bauxite deposition, ferralitic weathering products accumulated on the karst surface, and depressions began to develop. (B) During low GWT intervals, weathered materials in the karst depressions underwent intense leaching and bauxitization. (C) During high GWT intervals, weathered materials were submerged and the bauxitization process weakened. (D) Bauxitization was terminated by an Early Permian marine transgression, ending subaerial exposure of the Zunyi area.

of swamps on the karstified landscape, chemical weathering and leaching processes were weakened, and bauxitic claystone layers formed. Deepening of karstic depressions largely ceased during these intervals (Fig. 10C). 4) Multiple GWT cycles resulted in alternating layers of bauxite ore and bauxitic claystone as karst depressions deepened. After a major mid-Early Permian transgression marking the end of major LPIA glaciation, bauxitization at Zunyi ceased and the existing deposits were covered by marine strata (Fig. 10D).

7. Conclusions

(1) The Lower Carboniferous Jiujialu Formation bauxite deposits at Zunyi, northern Guizhou represent a karst bauxite deposit of the Kazakhstan subtype, marked by great thickness (to 110 m) and alternation of bauxite ore layers and bauxitic claystone (coal) layers. Rapid lateral changes in the thickness of these deposits were controlled by the irregular topography of the karstified landscape.
(2) The bauxite ore layers and bauxitic claystone layers differ in composition: the ore layers are high in Al and Ce/Ce^* and low in Si and La/Yb_N and have diaspore as the main mineral component, whereas the claystone layers are low in Al and Ce/Ce^* and high in Si and La/Yb_N and have illite as the main mineral component.
(3) Cycles of formation of bauxite ores and bauxitic claystones were controlled by hydrological changes (i.e., fluctuations in the paleogroundwater table at Zunyi) driven by Early Carboniferous glacioeustasy. During intervals of low GWT, enhanced chemical weathering and vertical leaching under oxic conditions led to formation of bauxite ore layers. During intervals of high GWT, water-logged soils and weaker chemical weathering under suboxic or anoxic conditions led to deposition of bauxitic claystone layers.

Acknowledgments

Prof. Médard Thiry and another anonymous reviewer are thanked for their constructive suggestions, which have greatly improved the quality of this paper. This study was supported by the Project of the Karstic Science Research Center (NSFC), the National Natural Science Foundation of China No. 41802116, Fundamental Research Funds for the Central Universities, China University of Geosciences (Wuhan) No. CUG170684, State Key Laboratory of Biogeology and Environmental Geology, China University of Geosciences (No. GKZ15Y671) and the Research Project of Guizhou Bureau of Geology and Mineral Exploration and Development (2015-No.4).

Appendix A. Supplementary data

Supplementary data to this article can be found online at https://doi.org/10.1016/j.oregeorev.2018.10.014.

References

Bárdossy, G., 1982. Karst bauxites: bauxite deposits on carbonate rocks. In: Developments in Economic Geology. Elsevier, Amsterdam, pp. 184pp..
Bárdossy, G., 1994. Carboniferous to Jurassic bauxite deposits as paleoclimatic and paleogeographic indicators. In: Embry, A.F., Beauchamp, B., Glass, D.J. (Eds.), Pangea: Global Environments and Resources. Canadian Society of Petroleum Geologists Memoir, pp. 283–293.
Bárdossy, G., Combes, P.J., 1999. Karst bauxites: interfingering of deposition and palaeoweathering. In: Thiry, M., Simon-Coinçon, R. (Eds.), Palaeoweathering, Palaeosurfaces and Related Continental Deposits. Blackwell Publishing Ltd., Oxford, UK, pp. 189–206.
Berger, G., Velde, B., Aigouy, T., 1999. Potassium sources and illitization in Texas Gulf Coast shale diagenesis. J. Sediment. Res. 69 (1), 151–157.
BGMRGZP (Bureau of Geologic and Mineral Resource of Guizhou Province), 1987. Regional Geology of the Guizhou Province. Geological Press House, Beijing (in Chinese with English abstract).
Bogatyrev, B.A., Zhukov, V.V., Tsekhovsky, Y.G., 2009. Phanerozic bauxite epochs. Geol. Ore Deposits 51 (6), 456–466.
Boski, T., Herbosch, A., 1990. Trace elements and their relation to the mineral phases in the lateritic bauxites from southeast Guinea Bissau. Chem. Geol. 82, 279–297.
Boulangé, B., Carvalho, A., 1997. The bauxite of Porto Trombetas. USP FAPESP, and Paris, ORSTOM, Sao Paulo, pp. 55–73.
Braun, J.-J., Pagel, M., Herbilln, A., Rosin, C., 1993. Mobilization and redistribution of REEs and thorium in a syenitic lateritic profile: A mass balance study. Geochim. Cosmochim. Acta 57 (18), 4419–4434.
Braun, J.-J., Pagel, M., Muller, J.-P., Bilong, P., Michard, A., Guillet, B., 1990. Cerium anomalies in lateritic profiles. Geochim. Cosmochim. Acta 54 (3), 781–795.
Cao, X., Wu, P., Wang, Z., Li, B., Lou, M., 2012. Investigation on the relativity between terra rossa and overlying carbonate strata and its implication at Wudang District of Guiyang City. Earth Environ. 40 (1), 57–62 (in Chinese with English abstract).
Caputo, M.V., de Melo, J.H.G., Streel, M., Isbell, J.L., 2008. Late Devonian and Early Carboniferous glacial records of South America. In: Fielding, C.R., Frank, T.D., Isbell, J.L. (Eds.), Resolving the Late Paleozoic Ice Age. Geological Society of America Special Paper, pp. 161–173.
Chen, X., Rong, J., Zhou, Z., Zhang, Y., Zhan, R., Liu, J., Fan, J., 2001. The Qianzhong Uplift and the Yichang Uplift during the transition of Ordovician and Silurian in the Upper Yangtze Region. Chin. Sci. Bull. 46 (12), 1052–1056 (in Chinese with English abstract).
D'Argenio, B., Mindszenty, A., 1995. Bauxites and related paleokarst: tectonic and climatic event markers at regional unconformities. Eclogae Geol. Helv. 88 (3), 453–499.
Deng, X., Yang, K., Liu, Y., She, Z., 2010. Characteristics and tectonic evolution of Qianzhong Uplift. Earth Sci. Front. 17 (3), 79–89 (in Chinese with English abstract).
Elliott, W.C., Haynes, J.T., 2002. The chemical character of fluids forming diagenetic illite in the Southern Appalachian Basin. Am. Mineral. 87 (11–12), 1519–1527.
Fedo, C.M., Nesbitt, W.H., Young, G.M., 1995. Unraveling the effects of potassium metasomatism in sedimentary rocks and paleosols, with implications for paleoweathering conditions and provenance. Geology 23 (10), 921–924.
Fielding, C.R., Frank, T.D., Isbell, J.L., 2008. The late Paleozoic ice age—A review of current understanding and synthesis of global climate patterns. In: Fielding, C.R., Frank, T.D., Isbell, J.L. (Eds.), Resolving the Late Paleozoic Ice Age. Geological Society of America Special Paper, pp. 343–354.
Gao, D., Sheng, Z., Shi, S., Cheng, L., 1992. Studies on the Bauxite Deposit in Central Guizhou, China. Guizhou Science and Technology Publishing House, Guiyang, pp. 151.
Gao, L., Li, J., Wan, D., Xiong, X., Yi, C., Han, M., 2015. Outline of metallogenic regularity of bauxite deposits in China. Acta Geol. Sin.-English Ed. 89 (6), 2072–2084.
Harnois, L., 1988. The CIW index: a new chemical index of weathering. Sed. Geol. 55, 319–322.
Kalaitzidis, S., Siavalas, G., Skarpelis, N., Araujo, C.V., Christanis, K., 2010. Late Cretaceous coal overlying karstic bauxite deposits in the Parnassus-Ghiona Unit, Central Greece: coal characteristics and depositional environment. Int. J. Coal Geol. 81 (4), 211–226.
Liao, S., Liang, T., 1991. Bauxite Geology of China. Science and Technology Publishing House of Guizhou, Guiyang, China (in Chinese with English abstract).
Ling, K.Y., Zhu, X.Q., Tang, H.S., Wang, Z.G., Yan, H.W., Han, T., Chen, W.Y., 2015. Mineralogical characteristics of the karstic bauxite deposits in the Xiuwen ore belt, Central Guizhou Province, Southwest China. Ore Geol. Rev. 65, 84–96.
Ling, K.Y., Zhu, X.Q., Tang, H.S., Li, S.X., 2017. Importance of hydrogeological conditions during formation of the karstic bauxite deposits, Central Guizhou Province, Southwest China: a case study at Lindai deposit. Ore Geol. Rev. 82, 198–216.
Liu, C., Jarochowska, E., Du, Y., Vachard, D., Munnecke, A., 2015. Microfacies and carbon isotope records of Mississippian carbonates from the isolated Bama Platform of Youjiang Basin, South China: possible responses to climate-driven upwelling. Palaeogeogr. Palaeoclimatol. Palaeoecol. 438, 96–112.
Liu, J.S., Algeo, T.J., Qie, W.K., Saltzman, M.R., 2018. Intensified oceanic circulation during Early Carboniferous cooling events: evidence from carbon and nitrogen isotopes. Palaeogeogr. Palaeoclimat. Palaeoecol in press.
Liu, P., 1991. Another discussion on Guizhou bauxite deposits-A study of Houcao bauxite material resources according to chemical composition features. Geol. Guizhou 8 (4), 313–321 (in Chinese with English abstract).
Liu, P., Liao, Y., 2012. A tentative discussion on the age of bauxite-bearing rock series in Central Guizhou-Southern Chongqing area. Geol. China 39 (3), 661–682 (in Chinese with English abstract).
Liu, P., Liao, Y., Zhang, Y., 2016. Sedimentary characteristics of sedimentary bauxite and ore-bearing rock series in corroded depression: a case study of the Houcao mining area in Zunyi. Geol. China 43 (2), 546–563 (in Chinese with English abstract).
Liu, W., Xu, X., Yu, Q., 2011. Discussion on forming mechanism and evolution of the Central Guizhou Palaeouplift. Acta Sedimentol. Sin. 29 (4), 658–664.
Liu, X., Wang, Q., Deng, J., Zhang, Q., Sun, S., Meng, J., 2010. Mineralogical and geochemical investigations of the Dajia Salento-type bauxite deposits, western Guangxi, China. J. Geochem. Explor. 105 (3), 137–152.
Lucas, Y., 1997. The bauxite of Juruti. In: Carvalho, A., Boulangé, B., Melfi, A.J., Lucas, Y. (Eds.), Brazilian Bauxites. USP FAPESP, and Paris, ORSTOM, Sao Paulo, pp. 107–136.
MacLean, W.H., 1990. Mass change calculations in altered rock series. Miner. Depos. 25 (1), 44–49.
MacLean, W.H., Barrett, T.J., 1993. Lithogeochemical techniques using immobile elements. J. Geochem. Explor. 48 (2), 109–133.
McLennan, S.M., 1989. Rare earth elements in sedimentary rocks: influence of provenance and sedimentary processes. Geochemistry and Mineralogy of Rare Earth Elements. In: Lipin, B.R., McKay, G.H. (Eds.), Reviews in Mineralogy. Mineralogical Society of America, Washington, D.C., pp. 170–200.
Mindszenty, A., 2016. Bauxites: feedbacks of system Earth at greenhouse times. Geol. Croat. 69 (1), 79–87.
Mongelli, G., 1993. REE and other trace elements in a granitic weathering profile from "Serre", southern Italy. Chem. Geol. 103 (1–4), 17–25.
Mongelli, G., 1997. Ce-anomalies in the textural components of Upper Cretaceous karst

bauxites from the Apulian carbonate platform (southern Italy). Chem. Geol. 140 (1–2), 69–79.
Mongelli, G., Boni, M., Buccione, R., Sinisi, R., 2014. Geochemistry of the Apulian karst bauxites (southern Italy): chemical fractionation and parental affinities. Ore Geol. Rev. 63, 9–21.
Mongelli, G., Buccione, R., Sinisi, R., 2015. Genesis of autochthonous and allochthonous Apulian karst bauxites (Southern Italy): Climate constraints. Sed. Geol. 325, 168–176.
Montañez, I.P., 2016. A Late Paleozoic climate window of opportunity. In: Proceedings of the National Academy of Sciences (U.S.A.), pp. 2334–2336.
Moore, P.D., 1989. The ecology of peat-forming processes: a review. Int. J. Coal Geol. 12 (1), 89–103.
Nesbitt, H.W., Markovics, G., 1997. Weathering of granodioritic crust, long-term storage of elements in weathering profiles, and petrogenesis of siliciclastic sediments. Geochim. Cosmochim. Acta 61 (8), 1653–1670.
Nesbitt, H.W., Young, G.M., 1982. Early Proterozoic climates and plate motions inferred from major element chemistry of lutites. Nature 299 (5885), 715–717.
Nesbitt, H.W., Young, G.M., 1984. Prediction of some weathering trends of plutonic and volcanic rocks based on thermodynamic and kinetic considerations. Geochim. Cosmochim. Acta 48 (7), 1523–1534.
Nicholls, R.J., Cazenave, A., 2010. Sea-level rise and its impact on coastal zones. Science 328 (5985), 1517–1520.
Niu, X., Feng, C., Liu, J., 2007. Formation mechanism and time of Qianzhong Uplift. Mar. Origin Petrol. Geol. 12 (2), 46–50 (in Chinese with English abstract).
Price, G.D., Valdes, P.J., Sellwood, B.W., 1997. Prediction of modern bauxite occurrence: implications for climate reconstruction. Palaeogeogr. Palaeoclimatol. Palaeoecol. 131 (1–2), 1–13.
Qie, W., Zhang, X., Du, Y., Zhang, Y., 2011. Lower Carboniferous carbon isotope stratigraphy in South China: implications for the Late Paleozoic glaciation. Sci. China D: Earth Sci. 54 (1), 84–92.
Retallack, G.J., 2010. Lateritization and bauxitization events. Econ. Geol. 105 (3), 655–667.
Rotzoll, K., Fletcher, C.H., 2012. Assessment of groundwater inundation as a consequence of sea-level rise. Nat. Clim. Change 3 (5), 477–481.
Rudnick, R., Gao, S., 2003. Composition of the Continental Crust. In: Holland, H.D., Turekian, K.K. (Eds.), The Crust, Treatise on Geochemistry. Pergamon, Oxford, pp. 1–64.
Rygel, M.C., Fielding, C.R., Frank, T.D., Birgenheier, L.P., 2008. The magnitude of Late Paleozoic glacioeustatic fluctuations: a synthesis. J. Sediment. Res. 78, 500–511.
Tribovillard, N., Algeo, T.J., Lyons, T., Riboulleau, A., 2006. Trace metals as paleoredox and paleoproductivity proxies: an update. Chem. Geol. 232 (1–2), 12–32.
Trolard, F., Tardy, Y., 1987. The stabilities of gibbsite, boehmite, aluminous goethites and aluminous hematites in bauxites, ferricretes and laterites as a function of water activity, temperature and particle size. Geochim. Cosmochim. Acta 51 (4), 945–957.
Valeton, I., 1999. Saprolite-bauxite facies of ferralitic duricrusts on palaeosurfaces of former Pangea. In: Thiry, M., Simon-Coinçon, R. (Eds.), Palaeoweathering, Palaeosurfaces and Related Continental Deposits. Special Publication of International Association of Sedimentologists, pp. 153–188.
Wang, Q., Deng, J., Liu, X., Zhang, Q., Sun, S., Jiang, C., Zhou, F., 2010. Discovery of the REE minerals and its geological significance in the Quyang bauxite deposit, West Guangxi, China. J. Asian Earth Sci. 39 (6), 701–712.
Wang, Q., Deng, J., Zhang, Q., Liu, H., Liu, X., Wan, L., Li, N., Wang, Y., Jiang, C., Feng, Y., 2011. Orebody vertical structure and implications for ore-forming processes in the Xinxu bauxite deposit, Western Guangxi, China. Ore Geol. Rev. 39 (4), 230–244.
Wang, X., Jiao, Y., Du, Y., Ling, W., Wu, L., Cui, T., Zhou, Q., Jin, Z., Lei, Z., Weng, S., 2013a. Rare earth element (REE) mobility and Ce anomaly in bauxite deposit of Wuchuan-Zheng'an-Daozhen Area, Northern Guizhou, China. J. Geochem. Explor. 133, 103–117.
Wang, X., Qie, W., Sheng, Q., Qi, Y., Wang, Y., Liao, Z., Shen, S., Ueno, K., 2013b. Carboniferous and Lower Permian sedimentological cycles and biotic events of South China. In: Gąsiewicz, A., Słowakiewicz, M. (Eds.), Palaeozoic Climate Cycles: Their Evolutionary and Sedimentological Impact. Geological Society of London Special Publication, pp. 33–46.
Weng, S., Lei, Z., Zhao, S., Ran, Y., Wang, X., Zhu, C., 2011. Relation between richening, preserving and paleokarst landform of Xianrenyan bauxite deposit in Zunyi. Guizhou Geol. 28 (4), 260–264 (in Chinese with English abstract).
Yang, Z., Sun, Z., Yang, T., Pei, J., 2004. A long connection (750–380 Ma) between South China and Australia: paleomagnetic constraints. Earth Planet. Sci. Lett. 220 (3), 423–434.
Yin, K., Chen, Y., 2007. Geological characteristic and development and exploration foreground of potassium-bearing rock in the Vicinity of Zunyi. Guizhou Geol. 24 (4), 282–286 (in Chinese with English abstract).
Young, G.M., Nesbitt, H.W., 1998. Processes controlling the distribution of Ti and Al in weathering profiles, siliciclastic sediments and sedimentary rocks. J. Sediment. Res. 68 (3), 448–455.
Yu, W., Algeo, T.J., Yan, J., Yang, J., Du, Y., Huang, X., Weng, S., 2018. Climatic and hydrologic controls on upper Paleozoic bauxite deposits in South China. Earth-Sci. Rev. https://doi.org/10.1016/j.earscirev.2018.06.014.
Zarasvandi, A., Zamanian, H., Hejazi, E., 2010. Immobile elements and mass changes geochemistry at Sar-Faryab bauxite deposit, Zagros Mountains, Iran. J. Geochem. Explor. 107 (1), 77–85.
Zhu, R., Yang, Z., Wu, H., Ma, X., Huang, B., Meng, Z., Fang, D., 1998. Paleomagnetic constraints on the tectonic history of the major blocks of China duing the Phanerozoic. Sci. China D: Earth Sci. 41 (s2), 1–19.